High-resolution finite element schemes for an idealized Z-pinch implosion model

Matthias Möller[a], Dmitri Kuzmin[b], John N. Shadid[c]

[a] *Institute of Applied Mathematics (LS III), Dortmund University of Technology, Vogelpothsweg 87, D-44227, Dortmund, Germany*
[b] *Department of Mathematics, University of Houston, 651 Philip G. Hoffman Hall, Houston, TX 77204-3008, USA*
[c] *Computational Sciences R&D Group, Sandia National Laboratories, PO Box 5800 MS 0316, Albuquerque, NM 87185-0316, USA*

Abstract

A high-resolution finite element method is developed for numerical simulation of Z-pinch-like implosions using a phenomenological model for the magnetic drive source term. The momentum and energy equations of the Euler system are extended by adding radial body forces proportional to the concentration of a scalar tracer field. The evolution of the tracer is governed by an additional transport equation which is solved in a segregated fashion. The finite element discretization is stabilized using a linearized flux-corrected transport (FCT) algorithm. Scalar viscosity of Rusanov type is employed to construct the underlying low-order scheme. In the process of flux limiting, node-by-node transformations from the conservative to the primitive variables are performed to ensure that all quantities of interest (density, pressure, tracer) are bounded by the physically admissible low-order values. The performance of the proposed algorithm on fully unstructured meshes is illustrated by numerical results for a power law implosion in the $x - y$ plane.

Keywords: finite elements, flux-corrected transport, systems of conservation laws, shock hydrodynamics, Z-pinch implosion
2000 MSC: 65M60, 65Z05, 76M10

Email addresses: matthias.moeller@math.tu-dortmund.de (Matthias Möller), kuzmin@math.uh.edu (Dmitri Kuzmin), jnshadi@sandia.gov (John N. Shadid)

1. Introduction

In a typical experiment of the Z-machine operated by Sandia National Laboratories, a very large electric current (dozens of MA) with a characteristic rise time of about 100 ns is carried by a cylindrical array of fine metallic wires which ablate and produce a plasma. The current flowing through the conductor generates a strong azimuthal magnetic flux. The Lorentz force drives the plasma towards the axis of symmetry causing a rapid implosion. While the highly energetic plasma stagnates on axis, its kinetic energy is converted into thermal energy, which gives rise to an intense X-ray pulse [1].

Numerical simulation of Z-pinch magnetic implosions is a highly challenging task due to the complexity of the involved physical processes, large jumps in density and pressure, and extremely small time scales. Banks and Shadid [2] developed a phenomenological model for the magnetic drive source term which can be readily built into existing CFD codes for the Euler equations to generate Z-pinch-like implosions. In this paper, we solve the generalized Euler system using continuous finite elements, implicit time-stepping, and a linearized flux-corrected transport (FCT) algorithm [3, 4].

The basic idea behind FCT methods is remarkably simple. Given two conservative approximations of high and low order, the difference between the corresponding numerical solutions is decomposed into a sum of raw antidiffusive fluxes. Next, each flux is multiplied by a correction factor and added to the low-order solution. The flux limiter is designed to ensure that no new maxima and minima can form, and existing extrema cannot grow.

The application of FCT to inviscid flow models based on the conservative form of the Euler equations requires special care. The primary variables are the density, momentum, and total energy. However, it is also important to keep the pressure nonnegative. To this end, a node-by-node transformation to the primitive variables is carried out as proposed in [4]. This limiting strategy makes it possible to control the local maxima and minima of selected control variables (e.g., density, pressure). The change of variables affects only the calculation of correction factors which are applied to the conservative fluxes.

Building on the above work, we develop a high-resolution FEM-FCT scheme for idealized Z-pinch implosions. The time-dependent magnetic drive source term is incorporated into the right-hand side of the Euler equations. The tracer equation is solved separately. An outer iteration is employed to resolve the coupling between the Euler system and the transport problem and this makes the proposed semi-coupled algorithm simple and efficient.

2. Idealized Z-pinch implosion model

The phenomenological model developed by Banks and Shadid [2] for simulation of prototypical Z-pinch implosions represents a generalized 2D Euler system coupled with a scalar transport equation for a tracer field λ

$$\frac{\partial U}{\partial t} + \nabla \cdot \mathbf{F}(U) = S(\mathbf{v}, \rho\lambda), \qquad \frac{\partial(\rho\lambda)}{\partial t} + \nabla \cdot (\rho\lambda\mathbf{v}) = 0. \tag{1}$$

The vector of conservative variables U and the pair of fluxes $\mathbf{F} = (F^1, F^2)$ for each coordinate direction in the Euclidean space $\mathbb{R}^2$ are given by

$$U = \begin{bmatrix} \rho \\ \rho\mathbf{v} \\ \rho E \end{bmatrix}, \qquad \mathbf{F} = \begin{bmatrix} \rho\mathbf{v} \\ \rho\mathbf{v} \otimes \mathbf{v} + p\mathcal{I} \\ \rho E\mathbf{v} + p\mathbf{v} \end{bmatrix}. \tag{2}$$

The pressure p is related to the density ρ, velocity $\mathbf{v}$, and specific total energy E by the equation of state for an ideal polytropic gas (with $\gamma = 1.4$)

$$p = (\gamma - 1)\rho\left(E - 0.5|\mathbf{v}|^2\right). \tag{3}$$

The inviscid fluxes $\mathbf{F}$ are homogeneous functions of order one. Hence, their relation to the Jacobians $\mathbf{A} = \frac{\partial \mathbf{F}}{\partial U}$ is quasi-linear, i.e. $\mathbf{F}(U) = \mathbf{A}(U)U$.

The magnetic drive source term S affects the momentum and energy equations only. It is motivated by the thin-shell Lorentz force model [2]:

$$S = \begin{bmatrix} 0 \\ \mathbf{f} \\ \mathbf{f} \cdot \mathbf{v} \end{bmatrix}, \qquad \mathbf{f} = (\rho\lambda)\left(\frac{I(t)}{I_{\max}}\right)^2 \frac{\hat{\mathbf{e}}_r}{r_{\text{eff}}}. \tag{4}$$

The non-dimensional r-coordinate r_{eff} is used to measure the local strength of the source term. The singularity at $r = 0$ is removed with the definition

$$r_{\text{eff}} = \max(r/R_0, 10^{-4}), \tag{5}$$

where R_0 denotes the inner radius of the liner at initial time. With $I_{\max} = 1$, the time-dependent current drive $I(t) = \sqrt{12(1-t^4)t^2}$ produces the power law implosion $R(t) = 1 - t^4$. The value of $I(t)$ is set to zero for simulation times larger than the implosion time τ_{impl}, i.e. non-dimensional times $t > 1$. A detailed derivation of the implosion model and alternative definitions of the current drive $I(t)$ can be found in the original publication [2].

The scalar quantity $\rho\lambda$ which is convected by the velocity field of the Euler model is used to localize the application of the Lorentz force and to control its magnitude ($0 \leq \lambda \leq 1$). The coupled problem (1) is very sensitive to phase errors and requires a highly accurate resolution of the flow field.

3. Finite element approximation

In this section, we present the high- and low-order space discretizations of the continuous problem (1). Let $\{\varphi_i\}$ be a set of finite element basis functions associated with the vertices of the mesh. Within the framework of a group finite element formulation [5], the vector of conservative variables U and the corresponding flux function $\mathbf{F}(U)$ are approximated by

$$U_h = \sum_j U_j \varphi_j, \qquad \mathbf{F}_h = \sum_j \mathbf{F}_j \varphi_j, \tag{6}$$

where $\mathbf{F}_j = \mathbf{A}_j U_j$ due to the homogeneity property of the Euler equations.

The finite element approximations to $\rho\lambda$ and $\rho\lambda\mathbf{v}$ are defined similarly

$$(\rho\lambda)_h \approx \sum_j (\rho\lambda)_j \varphi_j, \qquad (\rho\lambda\mathbf{v})_h \approx \sum_j (\rho\lambda)_j \mathbf{v}_j \varphi_j. \tag{7}$$

Let $M_C = \{m_{ij}\}$ denote the consistent mass matrix and $\mathbf{C} = \{\mathbf{c}_{ij}\}$ be the discrete gradient operator. The standard Galerkin discretization yields

$$m_{ij} = \int_\Omega \varphi_i \varphi_j \, \mathrm{d}\mathbf{x}, \qquad \mathbf{c}_{ij} = \int_\Omega \varphi_i \nabla \varphi_j \, \mathrm{d}\mathbf{x}.$$

Inserting approximations (6) and (7) into the Galerkin weak form of (1), one obtains a system of semi-discretized equations that can be written as

$$\sum_j \left(m_{ij} \frac{\mathrm{d}U_j}{\mathrm{d}t} \right) = \sum_j K_{ij} U_j + Q_i, \tag{8}$$

$$\sum_j \left(m_{ij} \frac{\mathrm{d}(\rho\lambda)_j}{\mathrm{d}t} \right) = \sum_j k_{ij} (\rho\lambda)_j. \tag{9}$$

where $Q_i = \int_\Omega \varphi_i S \, \mathrm{d}\mathbf{x}$. The definition of K_{ij} and k_{ij} is as follows [6, 7]

$$K_{ij} = -\mathbf{c}_{ij} \cdot \mathbf{A}_j, \qquad k_{ij} = -\mathbf{c}_{ij} \cdot \mathbf{v}_j. \tag{10}$$

A well-known drawback of the standard Galerkin discretization is the lack of stability which gives rise to nonphysical oscillations (undershoots and overshoots). The traditional remedies to this problem include (i) row-sum mass lumping and (ii) adding a suitable amount of artificial diffusion.

The lumped counterpart of the consistent mass matrix M_C is defined as

$$M_L = \text{diag}\{m_i\}, \qquad m_i = \sum_j m_{ij}. \tag{11}$$

In the case of a scalar transport equation, artificial diffusion should eliminate all negative off-diagonal entries k_{ij} of the discrete transport operator [8]. As a generalization to hyperbolic systems, negative eigenvalues of all off-diagonal blocks K_{ij} should be removed by the artificial viscosity operator [9]. A viable approach to satisfy both criteria simultaneously is to employ Rusanov-like scalar dissipation proportional to the maximum characteristic speed [10, 11]

$$d_{ij} = \max\{|k_{ij}| + c_{ij},\, |k_{ji}| + c_{ji}\}, \tag{12}$$

where $c_{ij} = \sqrt{\mathbf{c}_{ij} \cdot \mathbf{c}_{ij} \frac{\gamma p_i}{\rho_i}}$ is a multiple of the local speed of sound at node i and k_{ij} is an entry of the discrete transport operator given by (10).

The common discrete diffusion operator $D = \{d_{ij}\}$ is applied to the lumped-mass Galerkin scheme to obtain the nonoscillatory low-order scheme

$$m_i \frac{\mathrm{d}U_i}{\mathrm{d}t} = \sum_j K_{ij} U_j + \sum_{j \neq i} d_{ij}[U_j - U_i] + Q_i, \tag{13}$$

$$m_i \frac{\mathrm{d}(\rho\lambda)_i}{\mathrm{d}t} = \sum_j k_{ij} (\rho\lambda)_j + \sum_{j \neq i} d_{ij}[(\rho\lambda)_j - (\rho\lambda)_i], \tag{14}$$

where only the nearest neighbors of node i contribute to the sums over $j \neq i$.

A less diffusive low-order scheme, such as Roe's approximate Riemann solver or its generalization to finite element discretizations on unstructured meshes [7, 9], might fail to suppress spurious oscillations when applied to the magnetic implosion problem. This is unacceptable since the entire flux limiting machinery relies on the assumption that the local extrema of the low-order solution constitute physically legitimate upper and lower bounds.

4. Semi-coupled solution algorithm

To achieve unconditional stability, the coupled ODE systems (13) and (14) are discretized in time by the Crank-Nicolson ($\theta = 0.5$) or backward Euler ($\theta = 1$) scheme. The result is a nonlinear algebraic system which must be linearized or solved iteratively. In this work, we employ a fractional-step

algorithm in which the Euler system and the scalar transport equation are solved separately. Given the initial data or an approximation $[U^n, (\rho\lambda)^n]$ from the previous time step, the low-order solution is updated as follows:

In an outer coupling loop: 0. Let $U^{(0)} = U^n$ and $(\rho\lambda)^{(0)} = (\rho\lambda)^n$.

1. Given an approximation $(\rho\lambda)^{(k)}$, solve the nonlinear Euler system

$$\begin{aligned} M_L \frac{U^{(k+1)} - U^n}{\Delta t} &= \theta \left[N(U^{(k+1)}) + Q(\mathbf{v}^{(k+1)}, (\rho\lambda)^{(k)}) \right] \\ &+ (1-\theta) \left[N(U^n) + Q(\mathbf{v}^n, (\rho\lambda)^n) \right]. \end{aligned} \tag{15}$$

2. Given the velocity vector $\mathbf{v}^{(k+1)}$, solve the linear tracer equation

$$M_L \frac{(\rho\lambda)^{(k+1)} - (\rho\lambda)^n}{\Delta t} = \theta L^{(k+1)} (\rho\lambda)^{(k+1)} + (1-\theta) L^n (\rho\lambda)^n. \tag{16}$$

The superscripts in parentheses refer to the number of the current outer iteration ($k = 0, 1, \ldots, \bar{k} - 1$). The vectors N and Q represent the right-hand side of the semi-discrete problem (13). Each nonlinear algebraic system (15) is solved iteratively by a fixed-point defect correction scheme. In a practical implementation, the following two-step approach is employed [7]:

$$\begin{aligned} &A^{(k+1,l)} \Delta U^{(l+1)} = R^{(k+1,l)}, \\ &U^{(k+1,l+1)} = U^{(k+1,l)} + \Delta U^{(l+1)}, \end{aligned} \qquad l = 0, 1, \ldots, \bar{l} - 1 \tag{17}$$

where $A^{(k+1,l)}$ is a 'preconditioner', and $R^{(k+1,l)}$ is the residual given by

$$\begin{aligned} R^{(k+1,l)} &= M_L U^n + (1-\theta) \Delta t \left[N(U^n) + Q(\mathbf{v}^n, (\rho\lambda)^n) \right] \\ &- M_L U^{(k+1,l)} - \theta \Delta t \left[N(U^{(k+1,l)}) + Q(\mathbf{v}^{(k+1,l)}, (\rho\lambda)^{(k)}) \right]. \end{aligned} \tag{18}$$

At the first defect correction step, the solution is initialized by $U^{(1,0)} = U^n$ for $k = 0$ and by $U^{(k+1,0)} = U^{(k,\bar{l})}$ for $k > 0$. The iteration process is terminated when the relative changes and/or the residual become sufficiently small.

A usable preconditioner for (17) is the block matrix $A = \{A_{ij}\}$ with [7]

$$A_{ij} = m_i \delta_{ij} I - \theta \Delta t (K_{ij} + d_{ij} I) \tag{19}$$

where I is the 4×4 identity matrix and δ_{ij} denotes the Kronecker delta. This low-order operator has favorable matrix properties and is easy to invert. A

further simplification is obtained by setting $A_{ij} := 0$ for $j \neq i$. The result is a block-diagonal preconditioner that decouples the Euler system into four scalar equations for the density $\rho = U_1$, momenta $(\rho v_1, \rho v_2) = (U_2, U_3)$, and specific total energy $\rho E = U_4$ that can be solved one after the other [7]

$$\begin{aligned} &A_{pp}^{(k+1,l)} \Delta U_p^{(l+1)} = R_p^{(k+1,l)}, && p = 1, \ldots, 4, \\ &U_p^{(k+1,l+1)} = U_p^{(k+1,l)} + \Delta U_p^{(l+1)}, && l = 0, 1, \ldots, \bar{l} - 1. \end{aligned} \tag{20}$$

This preconditioning strategy is suitable for computations with small time steps. It was used to obtain the numerical results presented in Section 7.

In the linearized equation (16), the tracer $\rho\lambda$ is passively convected by the velocity field calculated from the solution $U^{(k+1,\bar{l})}$ to the first subproblem. Hence, there is no need for iterative defect correction. The low-order operator L is assembled using definitions (10) and (12) to evaluate k_{ij} and d_{ij}, respectively. The updated distribution of the tracer is used to recalculate the source term Q of the Euler system at the next outer iteration, if any.

The converged solution $\mathbf{U}^{n+1} = [U^{(\bar{k},\bar{l})}, (\rho\lambda)^{(\bar{k})}]$ to the fully discrete version of the coupled problem (13)–(14) serves as initial data for the next time step. The time-stepping loop runs until the final simulation time is reached.

A fully coupled approach would require defect correction for a nonlinear system of five equations. This would increase the size of the matrices for each linear solve by a factor of 25. Another benefit of the semi-coupled solution strategy is the possibility of using the wealth of well-tested software components developed for the Euler equations and scalar transport problems.

5. Flux correction for coupled problems

The flux-corrected transport (FCT) algorithm makes it possible to remove excess numerical viscosity from the low-order solution and achieve higher resolution without creating spurious undershoots and overshoots. By construction, the difference between the high-order Galerkin solution $\mathbf{U}_i^H$ and the low-order predictor $\mathbf{U}_i^L$ admits the following representation [4]

$$m_i \mathbf{U}_i^H = m_i \mathbf{U}_i^L + \sum_{j \neq i} \dot{\mathbf{F}}_{ij}, \qquad \dot{\mathbf{F}}_{ji} = -\dot{\mathbf{F}}_{ij}, \tag{21}$$

where $\mathbf{U}_i = [\rho_i, (\rho\mathbf{v})_i, (\rho E)_i, (\rho\lambda)_i]^\intercal$, and $\dot{\mathbf{F}}_{ij}$ is the raw antidiffusive flux

$$\dot{\mathbf{F}}_{ij} = \left[m_{ij} \left(\frac{\mathrm{d}\mathbf{U}_i}{\mathrm{d}t} - \frac{\mathrm{d}\mathbf{U}_j}{\mathrm{d}t} \right) + d_{ij}(\mathbf{U}_i - \mathbf{U}_j) \right]. \tag{22}$$

In the FCT algorithm proposed by Kuzmin [3], this flux is approximated by

$$\mathbf{F}_{ij}^L = \Delta t \left[m_{ij}(\dot{\mathbf{U}}_i^L - \dot{\mathbf{U}}_j^L) + d_{ij}(\mathbf{U}_i^L - \mathbf{U}_j^L) \right]. \tag{23}$$

The nodal time derivatives $\dot{\mathbf{U}}_i^L$ and $\dot{\mathbf{U}}_j^L$ are given by equations (13)–(14) whose right-hand sides are evaluated using the low-order solution $\mathbf{U}^L$. It is also possible to neglect the contribution of the consistent mass matrix. However, mass lumping degrades the phase accuracy of finite element schemes, and therefore, it is not to be recommended for time-dependent problems.

In the process of flux limiting, each raw antidiffusive flux $\mathbf{F}_{ij}^L$ is multiplied by a solution-dependent correction factor $\alpha_{ij} \in [0, 1]$. To keep the FCT scheme conservative, the same correction factor is applied to $\mathbf{F}_{ji}^L = -\mathbf{F}_{ij}^L$. Adding the limited antidiffusive fluxes to the low-order solution, we get

$$m_i \mathbf{U}_i = m_i \mathbf{U}_i^L + \sum_{j \neq i} \alpha_{ij} \mathbf{F}_{ij}^L, \qquad \alpha_{ji} = \alpha_{ij}. \tag{24}$$

Flux correction for systems of conservation laws requires a careful choice of the variables to be constrained. The formula for α_{ij} must guarantee that all quantities of interest stay bounded by the local maxima and minima of the low-order solution. In this work, we use the FCT limiter proposed in [4].

Let u_i^L denote the low-order value of a selected control variable (e.g., density or pressure). If the corresponding antidiffusive increment f_{ij}^u might create an undershoot or overshoot at node i, it must be limited. In accordance with the FCT philosophy, the correction factors α_{ij} are chosen so that

$$m_i(u_i^{\min} - u_i^L) \leq \sum_{j \neq i} \alpha_{ij}^u f_{ij}^u \leq m_i(u_i^{\max} - u_i^L), \tag{25}$$

where $u_i^{\max}$ and $u_i^{\min}$ are the local maximum and minimum values of u^L, i.e.,

$$u_i^{\max} - u_i^L = \max_{j \neq i}(u_j^L - u_i^L), \qquad u_i^{\min} - u_i^L = \min_{j \neq i}(u_j^L - u_i^L). \tag{26}$$

A suitable generalization of Zalesak's FCT limiter [11, 12] is as follows [4]:

1. Compute the sums of positive/negative antidiffusive increments to node i

$$P_i^+ = \sum_{j \neq i} \max\{0, f_{ij}^u\}, \qquad P_i^- = \sum_{j \neq i} \min\{0, f_{ij}^u\}. \tag{27}$$

2. Compute the distance to a local extremum of the low-order predictor

$$Q_i^+ = u_i^{\max} - u_i^L, \qquad Q_i^- = u_i^{\min} - u_i^L. \tag{28}$$

3. Compute the nodal correction factors for the net increment to node i

$$R_i^+ = \min\left\{1, m_i Q_i^+ / P_i^+\right\}, \qquad R_i^- = \min\left\{1, m_i Q_i^- / P_i^-\right\}. \tag{29}$$

4. Define $\alpha_{ij}^u = \alpha_{ji}^u$ so as to satisfy the FCT constraints for nodes i and j

$$\alpha_{ij}^u = \min\{R_{ij}, R_{ji}\}, \qquad R_{ij} = \begin{cases} R_i^+, & \text{if } f_{ij}^u \geq 0, \\ R_i^-, & \text{if } f_{ij}^u < 0. \end{cases} \tag{30}$$

5. Apply α_{ij}^u to all components of the raw antidiffusive flux given by (23).

This algorithm extends the standard FCT limiter [6, 12] to the case of nonconservative variables such that the antidiffusive 'fluxes' are not skew-symmetric ($f_{ji}^u \neq -f_{ij}^u$). As a result, the FCT constraint (25) may be imposed not only on the conservative but also on the primitive variables (typically, the pressure). Note that the change of variables affects only the calculation of the correction factors α_{ij} for the conservative solution update (24).

In our experience, the density ρ, pressure p, and tracer $\rho\lambda$ are the best control variables for the magnetic implosion problem. The pressure values and increments are obtained using the node-based transformation [4]

$$p_i = (\gamma - 1)\left((\rho E)_i - \frac{|(\rho \mathbf{v})_i|^2}{2\rho_i}\right), \tag{31}$$

$$f_{ij}^p = (\gamma - 1)\left(\frac{|\mathbf{v}_i|^2}{2} f_{ij}^\rho - \mathbf{v}_i \cdot \mathbf{f}_{ij}^{\rho v} + f_{ij}^{\rho E}\right). \tag{32}$$

Since the generic FCT limiter (27)–(30) is only applicable to one variable at a time, a common correction factor α_{ij} must be defined for the constrained solution update (24). A viable approach is to compute the correction factors for individual control variables sequentially [4]. First, the correction factor $\alpha_{ij}^{\rho\lambda}$ for the tracer is calculated and applied to $\mathbf{F}_{ij}$. Then the density limiter is invoked to constrain the flux $\alpha_{ij}^{\rho\lambda}\mathbf{F}_{ij}$ if necessary. The result $\alpha_{ij}^{\rho}\alpha_{ij}^{\rho\lambda}\mathbf{F}_{ij}$ is passed to the pressure limiter, and the final correction factor becomes

$$\alpha_{ij} = \alpha_{ij}^p \alpha_{ij}^\rho \alpha_{ij}^{\rho\lambda}. \tag{33}$$

Obviously, the value of α_{ij} depends on the order in which the correction factors α_{ij}^u are calculated. However, the raw antidiffusive increments f_{ij}^u already includes the net effect of previous corrections. Thus, only fluxes that still violate the FCT design criterion (25) need to be constrained.

The equation of state (3) shows that the total energy cannot become negative if the positivity of densities and pressures is enforced by the flux limiter. Also, the tracer is guaranteed to be nonnegative. In our experiments for the magnetic implosion problem, the above limiting strategy has always produced positive results, in spite of the involved linearizations. Therefore, there was no need for the optional failsafe post-processing feature described in [4].

6. Initialization of solution values

The initialization process is rarely described in publications on numerical methods for conservation laws. To prevent shocks from moving at wrong speeds, it is essential to make sure that the total mass, momentum, and energy of the initial solution agree with the analytically prescribed initial values. The pointwise definition $\mathbf{U}_i^0 = \mathbf{U}_0(\mathbf{x}_i)$ is generally nonconservative. Instead, the solution can be initialized using the Galerkin L^2 projection

$$\sum_j m_{ij}\mathbf{U}_j^H = \int_\Omega \varphi_i \mathbf{U}_0(\mathbf{x})\,\mathrm{d}\mathbf{x}. \tag{34}$$

Since $\sum_i \varphi_i \equiv 1$, this initialization technique preserves the 'mass' of the exact initial profile $\mathbf{U}_0(\mathbf{x})$. However, undershoots and overshoots may occur near steep fronts. To rectify this, row-sum mass lumping is commonly employed

$$m_i\mathbf{U}_i^L = \int_\Omega \varphi_i \mathbf{U}_0(\mathbf{x})\,\mathrm{d}\mathbf{x}. \tag{35}$$

The accuracy of the lumped-mass L^2 projection $\mathbf{U}^L$ can be improved using FCT [4]. By construction, the difference between the nodal values of $\mathbf{U}^H$ and $\mathbf{U}^L$ admits a conservative flux decomposition of the form (21) with

$$\mathbf{F}_{ij} = m_{ij}(\mathbf{U}_i^H - \mathbf{U}_j^H). \tag{36}$$

Following the algorithmic steps of the flux correction scheme for the coupled implosion model, Zalesak's limiter is used to impose the FCT constraint (25) on the density, pressure, and $\rho\lambda$. The synchronized correction factor α_{ij} is calculated from (33), and the final solution update is given by (24).

7. Numerical results

The presented FEM-FCT algorithm was applied to the thin-shell implosion problem [2] in the circular domain $\Omega = \{\mathbf{x} \in \mathbb{R}^2 : \|\mathbf{x}\| \leq 1.5\}$. In this experiment, the initial value of the tracer variable λ equals 1 if $1.0 \leq r \leq 1.05$ and $\lambda = 0$ otherwise. In contrast to the original publication [2], the solution to the Euler equations is initialized by the non-dimensional data

$$\rho' = \begin{cases} 1.0 & \text{if} \quad r < 1, \\ 10^6 & \text{if} \quad 1 \leq r \leq 1.05, \\ 0.5 & \text{if} \quad r > 1.05, \end{cases} \qquad \mathbf{v}' = 0.0, \qquad p' = 1.0. \tag{37}$$

These values serve as inflow boundary conditions which are imposed on $\partial\Omega$.

In the inner circle ($r \leq 0.5$), simulation is performed on a fully unstructured mesh with 7,164 triangles. A structured grid of 14,400 quadrilaterals is employed elsewhere ($0.5 \leq r \leq 1.5$). For illustration purposes, only a quarter of the mesh is depicted in Fig. 1 (a) along with the initial density profile.

The numerical results depicted in the symmetry plots Fig. 1 (c)–(d) were calculated using the Crank-Nicolson time-stepping scheme with $\Delta t = 10^{-5}$. The low-order scheme (marked by blue '+') leads to strong smearing of the liner, whereas the FCT limiter applied to the density, pressure, and tracer fields reproduces steep gradients with crisp resolution. Use of the consistent mass matrix improves the phase accuracy and leads to significantly larger density values (red and green '+'). In both cases, the synchronization of correction factors was performed by formula (33). Remarkably, radial symmetry is preserved in the structured and unstructured mesh regions for all three schemes even beyond the critical implosion time $t_{\text{impl}} = 1$ after which the density profile expands again. Moreover, all relevant quantities (density, pressure, energy, tracer) remain nonnegative. Therefore, no additional failsafe postprocessing was used. The temporal evolution of the inner shell radius is illustrated in Fig. 1 (b). Each marker '$\times$' represents the location of the vertex nearest to the origin whose density value is 1/2 of the maximum density at that time [2]. The so-defined shell radii of the numerical results are in good agreement with the exact solution $R(t) = 1 - t^4$ for $0 \leq t \leq 1$.

8. Conclusions

This paper sheds some light on the design of high-resolution finite element schemes for simulation of idealized implosions. Various algorithmic components that had originally been developed for scalar conservation laws [8, 6, 3]

(a) Initial density profile

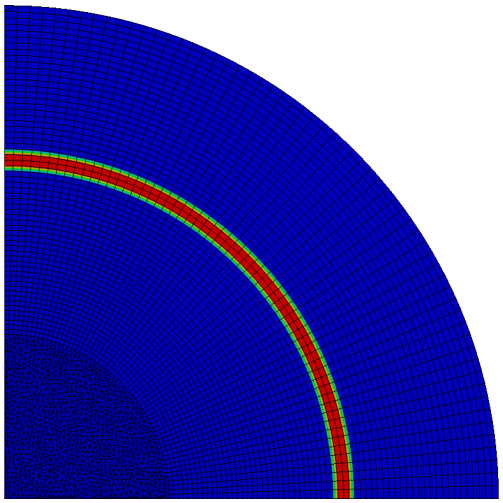

(b) Shell radius against time

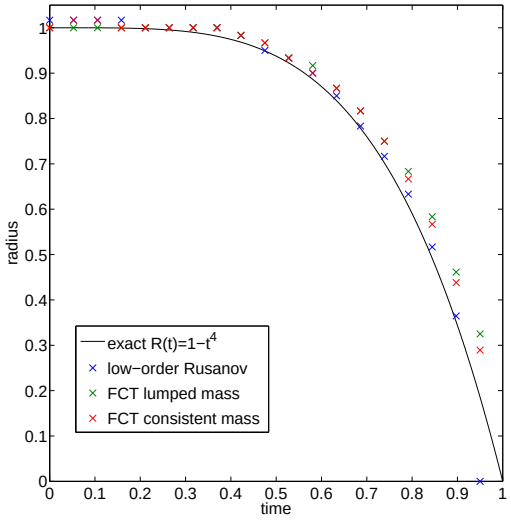

(c) Symmetry plot, $t = 0.9$

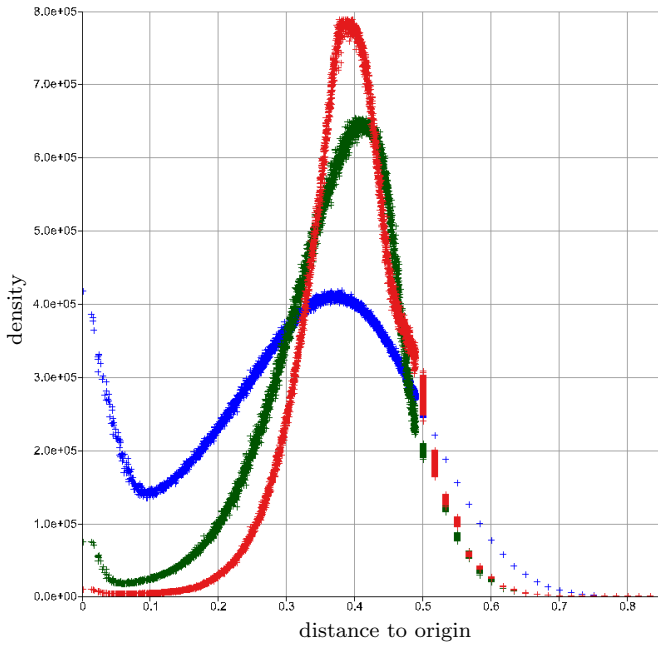

(d) Symmetry plot, $t = 1.05$

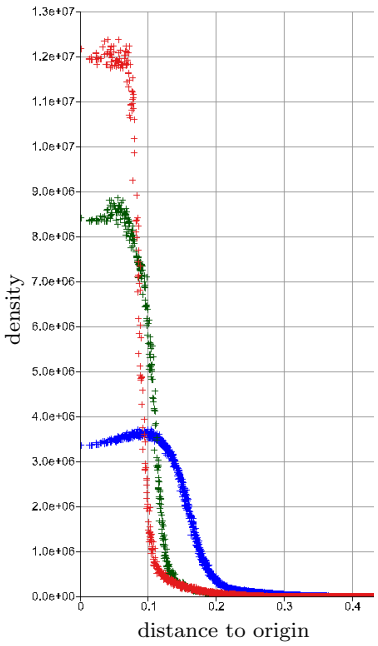

Figure 1: Power law implosion in the $x - y$ plane.

and for the compressible Euler equations [7, 9, 4] were reviewed and generalized to the prototypical Z-pinch implosion model proposed in [2]. In spite of its appearance, this model is *not* just an inhomogeneous Euler system combined with a scalar tracer equation. It should be treated as a strongly coupled system of conservation laws. This fact dictates the use of common artificial viscosities and synchronized flux limiting. However, the semi-coupled solution strategy turns out to be very efficient since only the Euler system gives rise to a nonlinear problem, while the tracer is updated by linear iterations.

The above splitting into two subproblems is particularly useful in the context of the linearized FEM-FCT scheme. The employed limiting strategy makes it possible to enforce positivity preservation not only for the conservative variables but also for other quantities. In contrast to classical FCT algorithms for systems, the change of variables is performed node-by-node rather than edge-by-edge. This approach is more robust than edge-based linearizations about an intermediate state. Indeed, averaging nodal values that differ by more than six orders of magnitude is likely to produce unbounded solutions. This problem can only be cured with the failsafe repair option.

References

[1] J. Chittenden, The Z-pinch approach to fusion, Physics World 13 (5) (2000) 39–43.

[2] J. Banks, J. Shadid, An Euler source term that develops prototype Z-pinch implosions intended for the evaluation of shock-hydro methods, Internal. J. Numer. Methods Fluids 61 (7) (2008) 725–751.

[3] D. Kuzmin, Explicit and implicit FEM-FCT algorithms with flux linearization, J. Comput. Phys. 228 (7) (2009) 2517–2534. doi:http://dx.doi.org/10.1016/j.jcp.2008.12.011.

[4] D. Kuzmin, M. Möller, J. Shadid, M. Shashkov, Failsafe flux limiting and constrained data projection for systems of conservation laws, Tech. Rep. 407, TU Dortmund, submitted to J. Comput. Phys. (2010).

[5] C. Fletcher, The group finite element formulation, Comput. Methods Appl. Mech. Engrg. 37 (1983) 225–243.

[6] D. Kuzmin, M. Möller, Algebraic flux correction I. Scalar conservation laws, in: D. Kuzmin, R. Löhner, S. Turek (Eds.), Flux-Corrected Transport, Principles, Algorithms, and Applications, Springer, 2005, pp. 155–206.

[7] D. Kuzmin, M. Möller, Algebraic flux correction II. Compressible Euler equations, in: D. Kuzmin, R. Löhner, S. Turek (Eds.), Flux-Corrected Transport, Principles, Algorithms, and Applications, Springer, 2005, pp. 207–250.

[8] D. Kuzmin, S. Turek, Flux correction tools for finite elements, J. Comput. Phys. 175 (2) (2002) 525–558.

[9] D. Kuzmin, M. Möller, S. Turek, High-resolution FEM-FCT schemes for multidimensional conservation laws, Comput. Methods Appl. Mech. Engrg. 193 (45–47) (2004) 4915–4946.

[10] J. Banks, W. Henshaw, J. Shadid, An evaluation of the FCT method for high-speed flows on structured overlapping grids, J. Comput. Phys. 228 (15) (2009) 5349–5369.

[11] S. Zalesak, The design of flux-corrected transport (FCT) algorithms for structured grids, in: D. Kuzmin, R. Löhner, S. Turek (Eds.), Flux-Corrected Transport: Principles, Algorithms, and Applications, Springer, 2005, pp. 29–78.

[12] S. Zalesak, Fully multidimensional flux-corrected transport algorithms for fluids, J. Comput. Phys. 31 (1979) 335–362.